First- and second-order phase transitions in a driven lattice gas with nearest-neighbor exclusion

Ronald Dickman*
Departamento de Física, ICEx, Universidade Federal de Minas Gerais, 30123-970 Belo Horizonte, MG, Brazil
(Received 12 February 2001; published 25 June 2001)

A lattice gas with infinite repulsion between particles separated by $\leqslant 1$ lattice spacing, and nearest-neighbor hopping dynamics, is subject to a drive favoring movement along one axis of the square lattice. The equilibrium (zero drive) transition to a phase with sublattice ordering, known to be continuous, shifts to lower density, and becomes discontinuous for large bias. In the ordered nonequilibrium steady state, both the particle and order-parameter densities are nonuniform, with a large fraction of the particles occupying a jammed strip oriented along the drive. The drive thus induces separation into high- and low-density regions in a system with purely repulsive interactions. Increasing the drive can provoke a transition to the ordered phase, and thereby, a sharp *reduction* in current.

DOI: 10.1103/PhysRevE.64.016124 PACS number(s): 05.70.Ln, 05.10.Ln, 05.40.−a, 64.60.Ht

I. INTRODUCTION

The study of simple nonequilibrium lattice hopping models, such as the asymmetric exclusion process (ASEP), has blossomed over the past decade, motivated by studies of traffic and of granular matter [1–7]. In parallel, there is continuing interest in *driven diffusive systems* (DDS): lattice gases with biased hopping [8–11], originally proposed as models of fast ionic conductors (FIC) [12]. These systems exhibit a variety of far-from-equilibrium collective phenomena, such as synchronization, jamming, and anisotropic phase separation.

In the widely studied case of DDS with attractive nearest-neighbor (NN) interactions, application of a driving field E (favoring hopping along one of the principal lattice directions) causes the interface between phases to orient along the field. Since the critical temperature increases with E, the drive favors ordering. In DDS with *repulsive* NN interactions, which is more pertinent to ionic conduction [13], ordering is generally associated with unequal sublattice occupation (as in antiferromagnetic spin systems), and one expects the drive to suppress order. Indeed, the original field theoretic, simulation, and mean-field analyses [14,15], showed that antiferromagnetic order is destroyed generically for a drive $E>2J$, J being the magnitude of the nearest-neighbor interaction. More recent simulations [16,17], using larger lattices, strongly suggest that global antiferromagnetic order is destroyed by *any* drive, however small. The observation that FIC materials exhibit phase transitions, even in the presence of repulsive short-range interactions, and growing interest in transport in particle systems, motivate investigation of a driven system with *hard-core* repulsion.

It will be shown that ordering in the case of infinite repulsion is much more robust than for the finite-repulsion DDS studied previously. While this accords with intuition, it is by no means obvious (one can still envision the finite-domain scenario, as found for finite J). Not only does the ordered state persist under driving, but it exhibits, in addition to sublattice ordering, a global separation into dense and dilute phases. This spontaneous spatial ordering is somewhat similar to ''lane-formation'' or ''flocking'' phenomena observed in systems of self-propelled agents [18,19], but here is intimitely connected with the existence of jammed states. Increasing the drive can provoke jamming, and thereby, a sharp reduction in the current, quite contrary to the usual relation between bias and current. (The system, in other words, exhibits negative differential resistance in some regions of parameter space.) The order of the phase transition, moreover, changes as the drive is increased. Thus, one finds a variety of surprising collective phenomena in a simple system.

The remainder of this paper is organized as follows. In the next section, I define the model and review its equilibrium properties. Section III presents simulation results pertinent to the phase diagram, while in Sec. IV, the mechanism of the phase transition is examined, and some results on dynamics are reported. Section V contains a summary and discussion. Several cluster-approximation results cited in the text are derived in the appendix.

II. MODEL

I study a lattice gas with occupancy of nearest-neighbor sites excluded (NNE): the distance between any pair of particles must be >1 lattice spacing; there are no other interactions. If we define an energy function on lattice configurations so:

$$E(\{\sigma\}) = J\sum_{NN} \sigma_i \sigma_j , \tag{1}$$

where the sum is over nearest-neighbor pairs, $\sigma_i = 0$ (1) in case site i is vacant (occupied), and $\{\sigma\}$ denotes the particle configuration, then the NNE model represents the $J\to\infty$ limit.

Equilibrium properties of this lattice analog of the hard-sphere fluid were studied via series expansion in the 1960's, leading to the conclusion that (on bipartite lattices) the system undergoes a continuous phase transition at a critical density ρ_c, to a state with preferential occupancy of one sublattice; $\rho_c \simeq 0.37$ on the square lattice [20–22]. (The chemical

*Electronic address: dickman@fisica.ufmg.br

potential is the temperaturelike parameter for this entropy-driven phase transition, which falls in the Ising universality class [21].)

The driven system follows a nearest-neighbor hopping dynamics. Each particle has an intrinsic rate of 1/4 for hopping in the $\pm y$ directions, and of $p/2$ and $(1-p)/2$ in the $+x$ and $-x$ directions, respectively. Denoting the intrinsic hopping rate by P, we have

$$P(i,j\rightarrow i,j\pm 1)=\frac{1}{4}, \tag{2}$$

$$P(i,j\rightarrow i\pm 1,j)=\frac{1}{4}\pm\frac{1}{2}\left(p-\frac{1}{2}\right). \tag{3}$$

Thus, $p-1/2$ represents the deviation from equilibrium, with $p=1$ corresponding to $E\rightarrow\infty$ in standard DDS. (Note, however, that in the present case, hard-core repulsion always takes precedence over the drive.)

I study the driven NNE lattice gas on a square lattice of L^2 sites, using periodic boundary conditions in both directions. Initially, N particles are thrown at random onto the lattice, respecting the NNE condition; this yields a homogeneous, disordered initial configuration. [The random sequential adsorption (RSA) or ''parking'' process used to generate the initial state eventually jams, at a mean density of 0.3641 [23]. In practice, one can reach densities up to about 0.38 for $L=100$.] In the dynamics, a randomly selected particle is assigned a hopping direction according to the rates given above, and the new position is accepted, subject to the NNE condition. N such attempted moves define one time unit. After a transient, whose duration depends upon p, L, and the density $\rho=N/L^2$, the system reaches a steady state in which the current density j (the net flux of particles along the $+x$ direction per site and unit time), and other macroscopic properties fluctuate about stationary values. I report results of extensive simulations at $p=1$, 0.75, and 0.6; some studies at $p=1/2$ were also performed to facilitate comparison with equilibrium. The simulations extend to a maximum time of from $\sim 3\times 10^6$ to $\sim 6\times 10^7$ steps, depending on the time required to reach the stationary state.

III. SIMULATION RESULTS: PHASE DIAGRAM

A. Current

To begin the analysis of the driven NNE system, I examine the stationary current density j. In a lattice gas with only onsite exclusion ($J=0$), $j\propto(2p-1)\rho(1-\rho)$. In the present case, we should again expect j to grow with ρ at low densities (increasing number of carriers) and to decrease at high density (increasing likelihood of blocking by occupied neighbors), but the maximum will move to $\rho<1/2$, since in the NNE system, each particle excludes five sites. These observations are verified in Fig. 1, which shows $j(\rho)$ for maximum drive, $p=1$. For $\rho\leqslant 0.25$ there is little dependence on system size; for the lower range of densities ($\rho\leqslant 0.1$) the simulation data are in good agreement with a four-site cluster mean-field calculation (see appendix). But at higher densities ($\rho=0.272$, 0.265, and 0.264 for $L=100$, 150, and 200, respectively), the current suddenly jumps to a lower value, and then continues to decrease smoothly with density. These data suggest a discontinuous phase transition (in the $L\rightarrow\infty$ limit) at a density $\rho_c\simeq 0.263$, far below that of the equilibrium critical point. Before analyzing the numerical evidence in greater detail, some observations are in order.

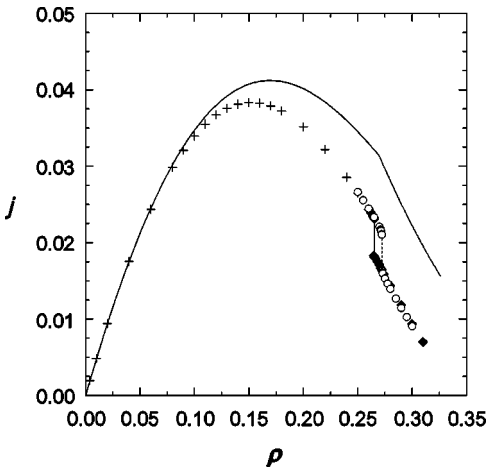

FIG. 1. Stationary current density versus particle density for $p=1$ and $L=50$ (+), $L=100$ (○), and $L=150$ (diamonds). Vertical lines indicate the transition at $L=100$ (dotted) and $L=150$ (solid). Solid curve: four-site MFT.

First, it is useful to examine a typical particle configuration in the high-density, low-current state; Fig. 2 shows such a snapshot, for $p=1$, $\rho=0.267$, and $L=200$, revealing a strongly nonuniform distribution: a high-density strip has formed parallel to the drive. Within the strip, all particles occupy a single sublattice, and their movement is blocked. The low-density region outside the strip shows no sublattice

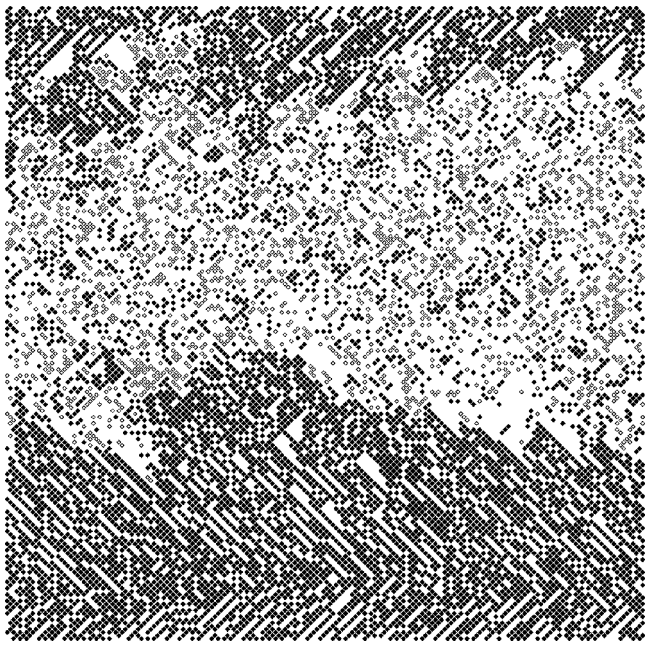

FIG. 2. Snapshot of particle configuration in stationary state, $p=1$, $\rho=0.267$, $L=200$. Filled and open symbols represent particles on different sublattices. Drive toward the right.

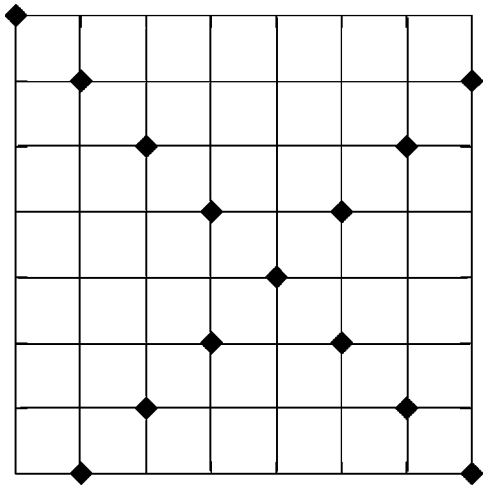

FIG. 3. Example of a low-density jammed configuration on a lattice with periodic boundaries. Such configurations are not encountered in simulations for $L \geqslant 50$.

ordering, and harbors all the mobile particles. (At first glance, the boundary between high- and low-density regions appears to be rough, but systematic studies of its width as a function of system size will be required to determine interface scaling properties.)

A second, related point is that the system exhibits *jammed states:* absorbing configurations in which each particle is blocked from moving by its neighbors (thus, $j=0$). Such configurations exist even at very low densities: an example is shown in Fig. 3. In practice, however, jammed states are not encountered in simulations for densities less than about 0.32, for $L \geqslant 150$ and $p=1$. In particular, jamming is never observed in the vicinity of the transition to the ordered phase. For $p=1$, jamming occurs readily if $\rho \geqslant 0.34$; in other words, the drive induces jamming at densities well below the RSA limit. A jammed configuration typical of the sort encountered in simulations is shown in Fig. 4. (Jammed states of the kind shown in Fig. 3, consisting of a small number of diagonal strips, were never observed in the simulations reported here, for which $L \geqslant 50$.) In jammed configurations, all particles occupy the same sublattice, but the particle density is essentially uniform, except for empty regions downstream from the point where a pair of diagonal rows of particles meet at a right angle. The system can jam for $p<1$ as well: while motion against the drive is possible in this case, particles queue up to form dense configurations whose lifetime grows exponentially with system size. For $p=0.75$ and $L=100$, jamming occurs at densities above about 0.37. (Note that the hopping dynamics employed here is reversible for $p=1/2$, so that the jammed configurations are then inaccessible.)

Jammed configurations are familiar from the *two species* driven lattice gas, with the two kinds of particle driven in opposite directions (and site exclusion the only interaction) [24,9]. In that case, jammed states form rather more readily than in the NNE lattice gas (for large driving fields the required density is ≈ 0.25), and are associated with a (possibly discontinuous) phase transition. Whether jamming represents a well-defined phase transition in the driven NNE system will be addressed in future work. Here, I concentrate on the

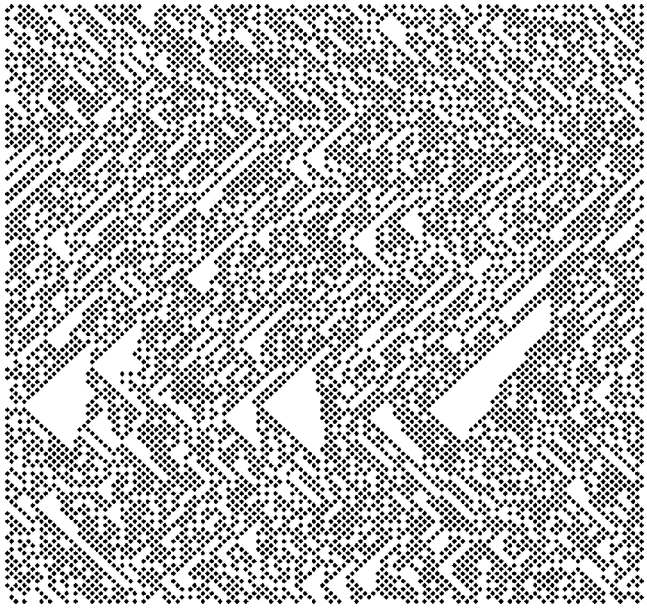

FIG. 4. Example of a jammed configuration, $p=1$, $\rho=0.34$, $L=150$. Drive toward the right.

phase transition between two *active* states, i.e., having a nonzero current. Jamming is nonetheless relevant to the nature of this transition, as discussed below.

Finally, one should note that the two- and four-site cluster mean-field theories (MFT), derived in the appendix, are so highly constrained by the NNE condition that the cluster probabilities are *independent* of the drive p. Pair MFT predicts a continuous transition to a sublattice-ordered state at $\rho_c=1/4$, while the four-site approximation shown in Fig. 1 gives $\rho_c=0.2696$. But since in equilibrium $\rho_c \simeq 0.37$, the fact that the kink in the MFT curve falls near the discontinuous transition should be seen as purely fortuitous. Larger clusters, or a spatially extended MFT will be needed to study the driven NNE lattice gas [25].

B. Order parameter

The phase transition in the NNE lattice gas is signaled by a nonzero order parameter

$$\phi = |\rho_A - \rho_B|, \tag{4}$$

where $\rho_i = N_i / L^2$, with N_i the number of particles in sublattice i.

Data for the stationary current and order parameter are obtained from histograms for the corresponding quantities, in the final (stationary) stage. Near the transition, at $p=1$ and 0.75, the histograms are bimodal (see Fig. 5).

Figure 6 shows the evolution of $j(t)$ and $\phi(t)$ in a single trial near ρ_c: the order parameter increases suddenly, after a long waiting time, and then jumps between high and low values. The current mirrors the changes in the order parameter, since the high value of the latter implies the presence of a strip of immobile particles. (The time to the onset of ordering varies from trial to trial, within the range $10^5 - 3 \times 10^6$, near ρ_c, for $p=1$ and $L=150$.)

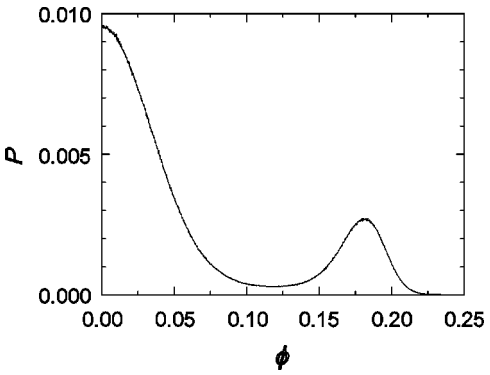

FIG. 5. Stationary order-parameter histogram, $p=1$, $\rho=0.2715$, $L=100$.

I report in Fig. 7 the stationary order parameter as a function of density for several values of the drive p. The phase transition is clearly discontinuous for $p \geqslant 0.75$, and continuous for $p=0.6$ and 0.5 (equilibrium). For $p=0.6$ the current is continuous in the vicinity of the transition (Fig. 8), and the system exhibits the hallmarks of a critical point: the variation of the order parameter with ρ becomes sharper with increasing system size; the histograms are unimodal, becoming very broad near the transition, so that the variance of the order parameter shows a sharp peak (Fig. 9), suggesting that $\chi \equiv L^2 var(\phi)$ (which represents the staggered susceptibility in equilibrium), will diverge as $L \to \infty$. Locating the *tricritical point*, at which the order of the transition changes, will require more extensive studies; the present results allow one to conclude that the tricritcal drive p_t lies between 0.6 and 0.75.

The transition from the disordered, high-conductivity state to the ordered, low-conductivity state occurs at lower density, the larger is p. Thus, we may cross the phase boundary at fixed density by augmenting p (Fig. 10); at this point the current, paradoxically, falls sharply in response to an increased drive.

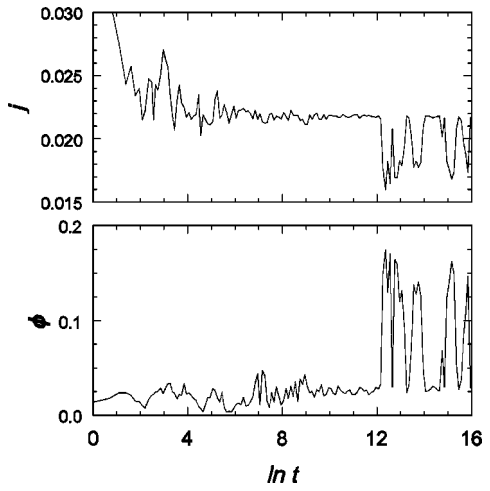

FIG. 6. Evolution of the order parameter (lower panel) and current density (upper) in a single trial for the same conditions as in Fig. 5.

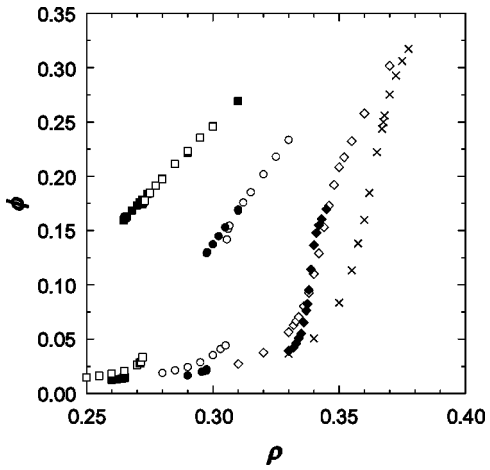

FIG. 7. Stationary order parameter versus density for $p=1$ (squares), $p=0.75$ (circles), and $p=0.6$ (diamonds). Open symbols are for $L=100$; filled, $L=150$. Crosses represent the equilibrium system ($p=1/2$) with $L=100$.

IV. TRANSITION MECHANISM: ORDERING VIA JAMMIMG

To understand the mechanism of the phase transition, we return to the particle configuration shown in Fig. 2. Within the high-density strip, as noted, particles are unable to move. Comparison of configurations at different times shows that while there are changes on the fringe, the interior of the strip is frozen on time scales of at least 10^4 steps.

For $p=1$ and 0.75, the strip normally contains a central core of maximum density, while the surrounding particles tend to fall along diagonal ''branches'' terminating on the core, forming a herringbone pattern, or, as it were, an arrow pointing along the drive. This suggests that the core forms first, and that particles are subsequently trapped along the branches. The growth of the latter is limited by reduction of the density outside the strip. For $p=0.6$, diagonal branches are again visible, but they are broader (5–10 lattice spacings).

While a detailed theory of the transition remains to be developed, it is possible to formulate a very simple theory of

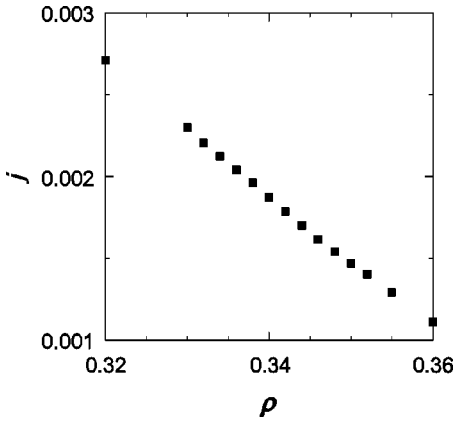

FIG. 8. Stationary current density j versus ρ for $p=0.6$ in the region of the transition; $L=100$.

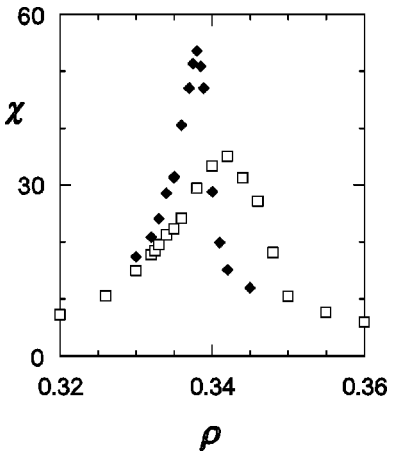

FIG. 9. $\chi \equiv L^2 \mathrm{var}(\phi)$ versus density for $p=0.6$ and $L=100$ (open symbols) and 150 (filled symbols).

branch dynamics. Imagine the branch as a diagonal sequence of particles terminating at the core, where no change is possible. The other ''free'' end is in contact with a region of uniform density ρ_0. Using the two-site approximation to estimate the rates of addition and loss of particles at the free end (see appendix), one finds that the branch grows for ρ_0 greater than 0.19, 0.26, and 0.29 in the neighborhood of the tip, for $p=1$, 0.75, and 0.6, respectively. (For smaller densities the tip shrinks.)

Figure 11 shows the density and order-parameter profiles perpendicular to the drive for the configuration of Fig. 2. The marked variation in the density indicates that a second order parameter (the difference between the maximium and minimum densities, $\Delta\rho=\rho_{max}-\rho_{min}$), can be associated with the phase transition. This density difference is *the* order parameter in DDS with attractive NN interactions, but in that case, the equilibrium system also shows phase separation, whereas the equilibrium NNE lattice gas does not have high- and low-density phases. In the NNE system, a nonzero $\Delta\rho$ is a uniquely nonequilibrium effect.

For $p=1$, ordered-state density profiles have $\rho_{max}\simeq 0.35$, essentially independent of ρ, while ρ_{min} generally falls the range 0.18–0.20, again without a systematic ρ dependence. For $p>1/2$, but less than unity, ordered configurations again show a high-density strip coexisting with a low-density region having a nonzero current and no sublattice ordering. For

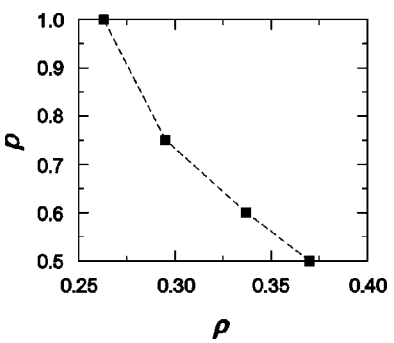

FIG. 10. Estimated phase boundary in the $\rho-p$ plane. Points represent simulation results; the lines are merely a guide to the eye.

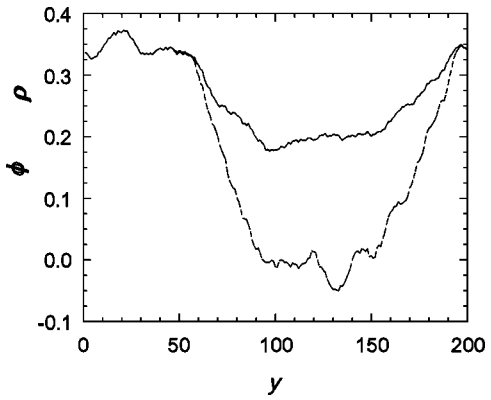

FIG. 11. Particle density (solid line) and order-parameter (broken line) profiles perpendicular to the field for the configuration shown in Fig. 2.

$p=0.75$, I find $\rho_{max}\simeq 0.383$, while for $p=0.6$, $\rho_{max}\simeq 0.40$. ρ_{min} also increases with decreasing p: $\rho_{min}\simeq 0.19$, 0.253, and 0.285 for $p=1$, 0.75, and 0.6, respectively, in reasonable agreement with the branch-growth model mentioned above.

Recall that for $p=1$, jamming occurs readily for $\rho \simeq 0.34$, that is, close to the density ρ_{max} of the jammed strip in the ordered state. Similarly, for $p=0.75$, the density in the strip is about 0.38, close to the global jamming density of 0.37 or so [26]. The strip, then, represents an instability to *local* jamming in a system whose density lies below that needed for global jamming. It is well known that driven particle systems such as the ASEP can exhibit a *shock*, i.e., a discontinuous density profile, which back propagates (in the direction opposite the drive) if the current in the high-density region is smaller than in the low-density region [5]. It is reasonable to suppose that such a shock forms in the present system due to a density fluctuation, and that its ''tail'' may then grow until it reaches the ''head,'' yielding a high-density ring that becomes the core of the jammed strip.

Once it has formed, additional particles cannot readily enter the jammed region, and so ρ_{max} does not vary with ρ. As the overall density ρ increases, ϕ grows (and j decreases) as a result of the expansion of the jammed region, which for sufficiently high density can fill the entire system.

I turn now to some results on dynamics. The apparent waiting time τ to the onset of the stationary state typically falls in the range 10^4–10^5 for $\rho<\rho_c$. At the transition, it shows a sharp maximum, 1–3 orders of magnitude above the pretransition value, and then falls off gradually [$\tau(\rho_c)\approx 2\times 10^6$ for $p=1$ and $L=150$]. Definitive results on relaxation times will require larger samples than were used in this study.

Another interesting observation is the appearance, in some realizations at $p=1$ and $\rho\geqslant 0.29$, of slow relaxation; examples are shown in Fig. 12. The order parameter grows roughly linearly with $\ln t$ over a sizeable interval before saturating. As in models of granular compaction [27] and of certain driven interfaces [28], this can be understood in terms of an exponential growth in the mean time between subsequent rearrangements, as the fully ordered state is approached. A model with purely excluded-volume interactions, but with rather different boundary and driving

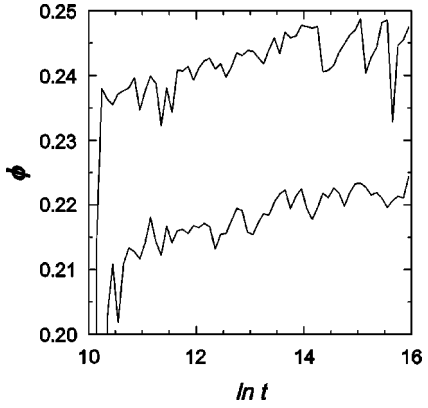

FIG. 12. Long-time evolution of the order parameter in two runs with $p=1$ and $L=150$. Upper curve, $\rho=0.30$; lower, $\rho=0.29$.

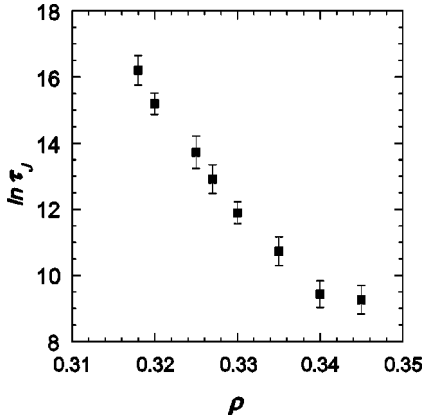

FIG. 13. Mean time to jamming versus density for $p=1$ and $L=150$.

conditions, has in fact been found to reproduce slow (logarithmic) granular compaction [29]. The present model may also be viewed as a ''scalar'' version of the situation envisioned in Ref. [30], in which application of a shear stress provokes jamming (and thus rigidity) in a granular medium.

As shown in Fig. 13, the mean-time τ_J to jamming exhibits an exponential dependence on the density. Studies at $p=1$ and $L=150$ give $\tau_J \simeq 10^4$ for $\rho \geqslant 0.34$, while for smaller densities τ_J grows exponentially with $(0.34-\rho)$, increasing by more than two orders of magnitude between $\rho=0.34$ and 0.32; τ_J exceeds the simulation time for $\rho<0.31$.

V. DISCUSSION

Imposing a bias on the hopping dynamics of a lattice gas with nearest-neighbor exclusion is found to favor antiferromagnetic ordering, in sharp contrast to what is observed in the case of finite repulsion, where the drive destroys order. The driven NNE lattice gas displays a surprisingly rich variety of behavior for its simplicity. The drive provokes separation into high- and low-density regions, despite the fact that all iteractions are repulsive. The transition becomes discontinuous for a sufficiently large bias.

A dynamic instability toward formation of a jammed, ordered region underlies these phenomena. That is, the combination of bias and hard-core exclusion leads to a situation in which the density in a region can increase until no further movement is possible. If such a region can grow to span the system (as evidently occurs at sufficiently high densities), then antiferromagnetic order is imposed globally, precluding the break-up into domains observed in the driven lattice gas with *finite* NN repulsion [16,17]. Thus, as in the attractive DDS, certain features of the ordered state can be understood on the basis of dynamic stability, as opposed to interactions or free-energy considerations. In the context of ASEP-like models, the results show that a two-dimensional system is capable of exhibiting a *bulk* phase transition, whereas the corresponding one-dimensional system is expected to show only *boundary-induced* transitions.

Jamming, i.e., the formation of locally or globally immobile configurations, is of great interest in the context of modeling colloidal dynamics [31,32], traffic [4], and granular media [6,7]. While the present model is too simple to represent such systems, it may yield insights into general aspects of jamming, for example, the dependence of the jamming probability or mean time to jamming on density and drive.

Many aspects of the system remain to be investigated. Related to the first-order phase transition is the question of hysteresis, and of the nucleation, growth, and decay of a jammed strip. The dynamics of the interface between high- and low-density regions should be of particular relevence to these issues. The nonequilibrium critical behavior observed for a smaller drive (e.g., $p=0.6$) is an important subject for a detailed study, since the nature of scaling in DDS remains controversial [9,10]. Further issues to be explored in future work are tricritical behavior; the effects of different initial configurations, of the aspect ratio (in rectangular systems), of boundary conditions (open along the drive, and/or reflecting perpendicular to it); temporal and spatial correlations, and finite-size effects. Finally, it would be very useful to develop continuum theoretical descriptions of this system, be they stochastic (Langevin-like, starting from a suitable time-dependent Landau-Ginzburg formulation), or deterministic (hydrodynamic, starting perhaps from a kinetic theory of the lattice model).

ACKNOWLEDGMENTS

I thank Martin Evans, Robin Stinchcombe, Gyorgy Szabó, Attila Szolnoki, Miguel A. Muñoz, and Hughes Chaté for helpful comments. This work was supported in part by CNPq and CAPES.

APPENDIX: CLUSTER APPROXIMATIONS

In this appendix I derive two- and four-site cluster approximations for the NNE lattice gas. (For background on

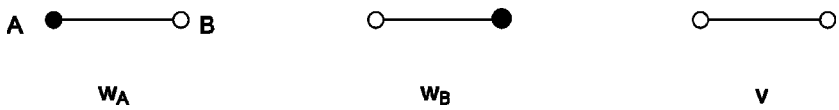

FIG. 14. Labeling scheme in the pair approximation.

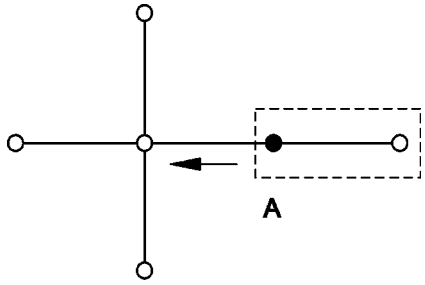

FIG. 15. An event contributing to the transition $w_A \to v$ as analyzed in the pair approximation.

cluster approximations for nonequilibrium lattice models, see Refs. [10] and [33].) In the two-site approximation we must consider the NN pairs shown in Fig. 14. The variables w_A, w_B and v represent the fraction of all NN pairs of the specified type, with the labels 'A' and 'B' denoting the sublattice. In a driven system we would, in general, have to distinguish between pairs oriented parallel and perpendicular to the drive. Here, however, the prohibition against NN occupied pairs implies that $w_i = \rho_i$ independent of orientation, where ρ_i ($i = A$ or B) is the fraction of occupied sites in sublattice i. (The overall particle density is $\rho = (\rho_A + \rho_B)/2$, while $v = 1 - \rho_B - \rho_B$.) Note as well that the placement of the sublattices is arbitrary: we could reverse the positions of A and B relative to the drive without altering the result.

In the two-site approximation we construct a closed set of equations for the pair probabilities by considering transitions among the NN states depicted in Fig. 14. Consider, for example, the transition shown in Fig. 15, where we assume the drive acts toward the right. The particle may exit horizontally (against the drive) or vertically; in either case the target site and its three neighbors not in the central pair must be vacant. In the two-site approximation we take the probability of such a configuration of six sites as $(w_A^2/\rho_A)[v/(1-\rho_B)]^3$. Here one factor of w_A represents the probability of the central pair, w_A/ρ_A is the probability of an occupied-vacant NN pair, given that the site in sublattice A is occupied, and the factors $v/(1-\rho_B)$ represent conditional probabilities for the neighbors of the target site to be vacant, given that the target site itself (which lies in the B-sublattice), is vacant. (Note that the NNE condition implies $w_A = \rho_A$, i.e., a site neighboring an occupied one *must* be vacant.) Including the intrinsic hopping rates, we find that the overall rate for transitions of this kind is

$$W(w_A \to v) = \rho_A \left(1 - \frac{p}{2}\right)\left(\frac{v}{1-\rho_B}\right)^3. \tag{A1}$$

Evaluating the remaining transition rates in the same manner, one readily obtains

$$\frac{d\rho_A}{dt} = v^3\left[\frac{\rho_B}{(1-\rho_A)^3} - \frac{\rho_A}{(1-\rho_B)^3}\right], \tag{A2}$$

and a similar equation for ρ_B (with subscripts A and B interchanged). Notice that p does not appear in these equations; the two-site approximation is insensitive to the drive. To study the possibility of ordering we consider solutions of the form $\rho_A = \rho + u$, $\rho_B = \rho - u$. A simple calculation shows that $u = 0$ is the only solution for $\rho < 1/4$, while for $\rho > 1/4$ we have in addition the ordered states

$$u = \pm(1-\rho)\left(\frac{4\rho - 1}{3 - 4\rho}\right)^{1/2}. \tag{A3}$$

Thus the pair approximation yeilds the usual kind of mean-field critical point, with the order-parameter exponent $\beta = 1/2$.

In the pair approximation the stationary current density is

$$j = \frac{v^3}{2}\left[\frac{p\rho_A}{(1-\rho_B)^3} - \frac{(1-p)\rho_B}{(1-\rho_A)^3}\right]. \tag{A4}$$

For $\rho < 1/4$ this yields

$$j = \rho\left(p - \frac{1}{2}\right)\left(\frac{1-2\rho}{1-\rho}\right)^3 \tag{A5}$$

while in the ordered state one finds

$$j = \left(p - \frac{1}{2}\right)\frac{3-4\rho}{8(1-\rho)^3}[1 - 6\rho + 12\rho^2 - 8\rho^3]. \tag{A6}$$

The current is continuous at the transition, and exhibits a maximum in the disordered state, for $\rho \simeq 0.1771$.

The cluster types considered in the *four-site* approximation are shown in Fig. 16. Once again, the positions of the sublattices relative to the drive are arbitrary and do not affect the final result. Symmetry forces equality between certain cluster densities: note for example that the density on sublattice A is given by

$$\rho_A = q_1 + q_5 = q_3 + q_5 \tag{A7}$$

implying that $q_3 = q_1$; similarly, $q_2 = q_4$.

Configuration probabilities are again approximated using conditional probabilities, given the presence of the central four-site cluster. The following examples illustrate the procedure. First consider a transition of a 4-site cluster from state 0 to state 1. The particle may enter the central cluster from the right or from below. The configuration required in the former case is shown in Fig. 17(a); we approximate its probability as $q_0 q_2/(1-\rho_A)$, that is, the probability of the central cluster times the conditional probability of a cluster

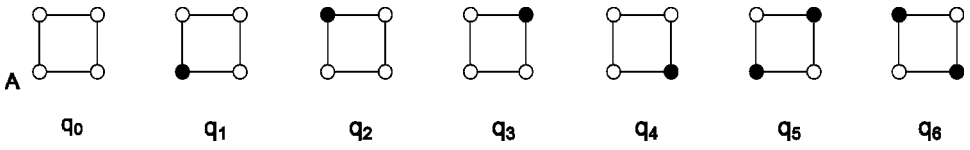

FIG. 16. Labeling scheme in the four-site approximation.

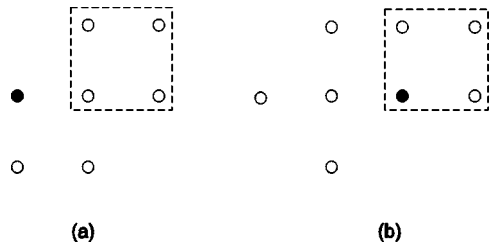

FIG. 17. (a) Configuration required for the transition $q_0 \to q_1$. (b) Configuration required for the reverse transition.

in state 2, given that one site (in sublattice A) is vacant. The *rate* of this process is $p/2+1/4$ times the preceding expression.

Now consider the reverse transition; the particle may exit to the left or below. The configuration required in the former case is given in Fig. 17b; its probability is approximated as

$$\frac{q_1^2}{\rho_A}\frac{q_0+q_2}{1-\rho_B},$$

where one factor of q_1 is due to the central cluster, a factor q_1/ρ_A represents the conditional probability of state 1, given one edge with its A-sublattice site occupied (and, by necessity, the adjacent B-sublattice site vacant). The final factor, $(q_0+q_2)/(1-\rho_B)$, is the conditional probability of a cluster in state 0 *or* 2, given one site (in the B-sublattice) vacant.

Enumerating the remaining transitions into and out of state 0 one obtains

$$\frac{dq_0}{dt} = -q_0\left(\frac{q_2}{v_B}+\frac{q_1}{v_A}\right)+\frac{q_1^2}{\rho_A}s_2+\frac{q_2^2}{\rho_B}s_1, \tag{A8}$$

where $v_i = 1-\rho_i$ $(i=A$ or $B)$, $s_1=(q_0+q_1)/v_A$, and $s_2 = (q_0+q_2)/v_B$. A similar analysis yields

$$\frac{dq_1}{dt} = \frac{1}{2}\left(q_2 s_1 - q_1 s_2 + \frac{q_2}{v_A}[q_0-q_1]+\frac{q_1 s_2}{\rho_A}[q_5-q_1]\right). \tag{A9}$$

The equation for q_2 is obtained by exchanging labels 1 and 2, 5 and 6, and A and B in the above. Finally, for state 5 one finds

$$\frac{dq_5}{dt} = q_1\left(\frac{q_2}{v_A}-\frac{q_5 s_2}{\rho_A}\right), \tag{A10}$$

with the corresponding equation for q_6 given by interchanging labels as before. Notice that p appears in none of these equations, i.e., the 4-site approximation is also insensitive to the nonequilibrium drive.

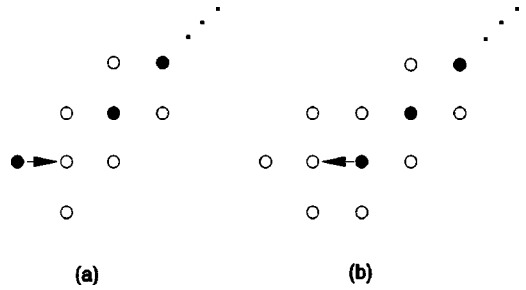

FIG. 18. (a) An event contributing to the growth of a branch; dots indicate the continuation of the branch, which terminates at the core. (b) An event contributing to the shrinkage of a branch.

Eqs. (A8)–(A10) are integrated numerically, using a fourth-order Runge-Kutta scheme [34]. The transition, which is again continuous, occurs at $\rho_c = 0.2696$, closer to the (equilibrium) critical density of 0.37 than in the 2-site approximation [25]. The current in the 4-site approximation, given by

$$j = \frac{2p-1}{4}(q_1 s_2 + q_2 s_1), \tag{A11}$$

is plotted in Fig. 1. While this prediction is in good agreement with simulations at low densities, the analysis must be extended to larger clusters to take the drive into account [25].

Finally, we apply the pair approximation to the growth and evaporation dynamics of a diagonal branch. Figure 18 depicts the situation around the free tip, in whose vicinity we assume a uniform density ρ_0, sufficiently low that there is no sublattice ordering. The other end of the branch is assumed to terminate at the core of the high-density strip; the branch can grow or shrink only at its free end. The addition event shown in Fig. 18a has, in the pair approximation, the rate $(p/2)\rho_0 v/(1-\rho_0)$ while for the corresponding event with motion perpendicular to the drive, the rate is $(1/4)\rho_0 v/(1-\rho_0)$. (Note that we regard the presence of the branch tip as given; thus its probability does not appear in these expressions.) The loss event shown in Fig. 18(b) has the rate $[(1-p)/2][v/(1-\rho_0)]^3$; the rate for the event in which the particle moves perpendicular to the drive is $(1/4)[v/(1-\rho_0)]^3$. If we let n represent the mean number of particles in the branch, then combining the gain and loss terms we find

$$\frac{dn}{dt} = \frac{1}{4}\frac{1-2\rho_0}{1-\rho_0}\left[(2p+1)\rho_0 - (3-2p)\left(\frac{1-2\rho_0}{1-\rho_0}\right)^2\right]. \tag{A12}$$

The density ρ_0 for which $dn/dt=0$ is interpreted as the stationary density near the branch tip.

[1] J. Krug, Phys. Rev. Lett. **67**, 1882 (1991).
[2] B. Derrida, M.R. Evans, V. Hakim, and V. Pasquier, J. Phys. A **26**, 1493 (1993).
[3] R.B. Stinchcombe and G.M. Schütz, Phys. Rev. Lett. **75**, 140 (1995); R.B. Stinchcombe, M.D. Grynberg, and M. Barma, Phys. Rev. E **47**, 4018 (1993).
[4] *Traffic and Granular Flow*, edited by D. E. Wolf and M. Schreckenberg (Springer-Verlag, Berlin, 1998).

[5] G. M. Schütz, in *Phase Transitions and Critical Phenomena*, edited by C. Domb and J. L. Lebowitz (Academic Press, London, 2000), Vol. 18.
[6] H.M. Jaeger, S.R. Nagel, and R.P. Behringer, Rev. Mod. Phys. **68**, 1259 (1996).
[7] L.P. Kadanoff, Rev. Mod. Phys. **71**, 435 (1999).
[8] S. Katz, J.L. Lebowitz, and H. Spohn, Phys. Rev. B **28**, 1655 (1983); J. Stat. Phys. **34**, 497 (1984).
[9] B. Schmittmann and R. K. P. Zia, *Statistical Mechanics of Driven Diffusive Systems*, Vol. 17 of *Phase Transitions and Critical Phenomena*, edited by C. Domb and J. L. Lebowitz (Academic Press, London, 1995).
[10] J. Marro and R. Dickman, *Nonequilibrium Phase Transitions in Lattice Models* (Cambridge University Press, Cambridge, 1999).
[11] T. Antal and G.M. Schütz, Phys. Rev. E **62**, 83 (2000).
[12] J.B. Boyce and B.A. Huberman, Phys. Rep. **51**, 189 (1979); W. Dieterich, P. Fulde, and I. Peschel, Adv. Phys. **29**, 527 (1980).
[13] While the crystal lattice may mediate an effective attractive contribution to the interaction, excluded volume and Coulombic forces should, in general yield, a net repulsion between ions of the same species, at short range.
[14] K.-t. Leung, B. Schmittmann, and R.K.P. Zia, Phys. Rev. Lett. **62**, 1772 (1989).
[15] R. Dickman, Phys. Rev. A **41**, 2192 (1990).
[16] G. Szabó, A. Szolnoki, and T. Antal, Phys. Rev. E **49**, 299 (1994).
[17] G. Szabó and A. Szolnoki, Phys. Rev. E **53**, 2196 (1996).
[18] D. Helbing, I.J. Farkas, and T. Vicsek, Phys. Rev. Lett. **84**, 1240 (2000).
[19] A. Czirók, M. Vicsek, and T. Vicsek, Physica A **264**, 299 (1999).
[20] L.K. Runnels and L.L. Combs, J. Chem. Phys. **45**, 2482 (1966).
[21] D.S. Gaunt and M.E. Fisher, J. Chem. Phys. **43**, 2840 (1965); D.S. Gaunt, *ibid.* **46**, 3237 (1967).
[22] F.H. Ree and D.A. Chesnut, J. Chem. Phys. **45**, 3983 (1966).
[23] P. Meakin, J.L. Cardy, E. Loh, and D.J. Scalapino, J. Chem. Phys. **86**, 2380 (1987); R. Dickman, J.-S. Wang, and I. Jensen, *ibid.*, **94**, 8252 (1991).
[24] B. Schmittmann, K. Hwang, and R.K.P. Zia, Europhys. Lett. **19**, 19 (1992).
[25] G. Szabó and A. Szolnoki (private communication) report that a more symmetric four-site approximation scheme yields a somewhat improved estimate for ρ_c, but still, with no dependence on the drive p. It appears from their analysis that clusters of at least five sites are required to demonstrate a nonzero p-dependence.
[26] For $p=0.6$, the jamming density can be estimated as about 0.40 from the density in the strip. This is beyond the density that can be prepared via RSA.
[27] E. Ben-Naim, J.B. Knight, and E.R. Nowak, Physica D **123**, 380 (1998).
[28] Y. Kafri, D. Biron, M.R. Evans, and D. Mukamel, Eur. Phys. J. B **16**, 669 (2000).
[29] E. Caglioti, V. Loreto, H.J. Herrmann, and M. Nicodemi, Phys. Rev. Lett. **79**, 1575 (1997).
[30] M.E. Cates, J.P. Wittmer, J.-P. Bouchaud, and P. Claudin, Phys. Rev. Lett. **81**, 1841 (1998).
[31] S.B. Santra, S. Schwarzer, and H. Herrmann, Phys. Rev. E **54**, 5066 (1996).
[32] O.J. O'Loan, M.R. Evans, and M.E. Cates, Physica A **258**, 109 (1998).
[33] A.G. Dickman, B.C.S. Grandi, W. Figueiredo, and R. Dickman, Phys. Rev. E **59**, 6361 (1999).
[34] W. H. Press, B. P. Flannery, S. A. Teukolsky, and W. T. Vetterling, *Numerical Recipes* (Cambridge University Press, Cambridge, 1986).